

Research Paper

Influence of maize picking roller surface structure on stalk pulling force



Yipeng Cui ^{a,b,c}, Pengxuan Guan ^{a,b,c}, Jianning Yin ^{a,b,c}, Zehao Zha ^{a,b,c}, Qiming Yu ^{a,b,c}, Zhenwei Wang ^d, Duanyang Geng ^{a,b,c,*}

^a School of Agricultural Engineering and Food Science, Shandong University of Technology, Zibo, 255091, PR China

^b Institute of Modern Agricultural Equipment, Shandong University of Technology, Zibo, 255091, PR China

^c Shandong Provincial Key Laboratory of Smart Agricultural Technology and Intelligent Agricultural Machinery and Equipment for Field Crops, Shandong University of Technology, Zibo, 255091, PR China

^d Nanjing Institute of Agricultural Mechanization, Ministry of Agriculture and Rural Affairs, Nanjing, 210014, PR China

ARTICLE INFO

ABSTRACT

Keywords:

DEM-MBD coupled simulation
Picking roller surface structure
Stalk pulling force
Ear-picking device
Maize stalk

During the maize ear harvesting process, a reasonable selection of the picking roller's surface structure can significantly enhance stalk pulling force, reduce ear-picking losses, and improve overall harvesting efficiency. Investigating the influence of different picking roller surface structures on stalk pulling force is therefore of critical importance. In this study, a simulation model was developed based on the Discrete Element Method (DEM) and Multi-Body Dynamics (MBD) to simulate the interaction mechanisms between the ear-picking device and maize stalks. The accuracy of the simulation model was validated through bench tests, using maximum stalk pulling force and power consumption as key evaluation metrics, with relative errors of 5.4 % and 5.2 %, respectively. The study further explored the effects of picking roller surface structure (pattern shape, pattern height and pattern spacing) on stalk pulling force. The results indicate that pattern shape, pattern height, pattern spacing, and their interactions have a significant impact on stalk pulling force. The optimal surface structure of the picking roller is an inclined pattern structure with a pattern height of 2.5 mm and a pattern spacing of 8 mm. The simulation results can be used to analyse the effect of the picking roller surface structure on stalk pulling force, providing a theoretical basis for the rational selection of picking roller surface structures.

Nomenclature

(continued)

DEM	Discrete element method
MBD	Multi-body dynamics
A	Particle contact area
d	Average radius of the picking roller (m)
E*	Equivalent young's modulus (Pa)
E ₁	Young's modulus of particle 1 (Pa)
E ₂	Young's modulus of particle 2 (Pa)
e	Coefficient of restitution
F ₁	Stalk pulling force (N)
F ₂	Compression force (N)
F _{max}	Maximum stalk pulling force (N)
F _n	Normal force (N)
F _n ^d	Normal damping force (N)
F _t	Tangential force (N)
F _t ^d	Tangential damping force (N)
G*	Equivalent shear modulus (Pa)
G ₁	Shear modulus of particle 1
G ₂	Shear modulus of particle 2

(continued on next column)

J	Moment of inertia
m*	Equivalent mass (g)
n	Rotational speed of the picking roller (r·min ⁻¹)
R*	Equivalent radius (m)
R ₁	Radius of particle 1 (m)
R ₂	Radius of particle 2 (m)
R _b	Bonding radius
r ₁	Position vectors of the centers of particle 1
r ₂	Position vectors of the centers of particle 2
S _n	Normal stiffness (N·m ⁻¹)
S _t	Tangential stiffness (N·m ⁻¹)
T	Real-time torque of the picking roller (N·m)
T _{max}	Maximum torque (N·m)
v _n	Normal velocity (m·s ⁻¹)
v _t	Tangential velocity (m·s ⁻¹)
v _n ^{vel}	Normal component of the relative velocity (m·s ⁻¹)
v _t ^{vel}	Tangential component of the relative velocity (m·s ⁻¹)
W	Power consumption (W)

(continued on next page)

* Corresponding author. School of Agricultural Engineering and Food Science, Shandong University of Technology, Zibo, 255091, PR China.

E-mail address: dygxt@sut.edu.cn (D. Geng).

(continued)

β	Coefficient related to the restitution coefficient
δF_n	Normal bonding force (N)
δF_t	Tangential bonding force (N)
δM_n	Normal moment (N·m)
δM_t	Tangential moment (N·m)
δ_n	Normal overlap between particles (m)
δ_t	Overlap coefficient (m)
δ_z	Time step
μ	Friction coefficient
ν_1	Poisson's ratios of particle 1
ν_2	Poisson's ratios of particle 2
σ_{\max}	Normal critical stress
τ_{\max}	Tangential critical stress
ω_n	Normal angular velocity (rad·s ⁻¹)
ω_t	Tangential angular velocity (rad·s ⁻¹)

1. Introduction

Vibration ear-picking is a technique that facilitates the separation of ears from stalks by applying high-frequency vibration during the stalk clamping and conveying process (Wang et al., 2018). Compared to conventional picking mechanisms, this approach avoids direct contact between the ear and the picking rollers, thereby reducing ear damage (Du et al., 2012; Qin et al., 2020). As the core component responsible for ear-stalk separation, the picking roller's ability to effectively grasp the stalk is a critical prerequisite for efficient ear detachment (Fu et al., 2023; Gang et al., 2016). The surface structure of the picking roller significantly influences both the stalk pulling force and the overall picking efficiency. Due to stalk compression deformation and juice exudation from high-moisture stalks during the ear-picking process, the clamping force exerted by the picking roller on the stalk undergoes substantial variations, leading to a marked reduction in stalk pulling force (J. Shinners et al., 2009; Seifi & Alimardani, 2010; Tai et al., 2021). Therefore, improving the picking roller's ability to reliably grip the stalk is the key to effectively transmitting both clamping force and high-frequency vibrations.

To address the issue of the clamping stability of picking rollers affects stalk pulling force, extensive research has been conducted. Introducing raised rib structures on the surface of picking rollers has been shown to effectively enhance the pulling force exerted on the stalk. However, these structures also intensify compressive damage to the stalk, frequently resulting in stalk breakage during operation (Dong et al., 2024; R. Yang et al., 2021; Zhang et al., 2022). In response to this challenge (Zhu et al., 2023), developed a bionic picking roller featuring regularly arranged protrusions on its surface. This design not only increases stalk pulling force but also mitigates stalk damage. Similarly (Xin et al., 2023), developed a vertical ear-picking device, which reduces ear damage during harvesting. However, its poor adaptability to stalk diameter leads to unstable stalk pulling force, frequently resulting in stalk breakage. Clearly, to enhance the reliability and operational quality of the ear-picking process, there is an urgent need to conduct in-depth research on effective methods to improve stalk clamping force. In addition, there is a lack of in-depth and systematic research on the problem of insufficient stalk pulling force of the picking rollers with excitation effect studied in this paper.

Ear-stalk separation through picking roller-stalk interactions is a complex transient process that is difficult to visualise. The primary reasons for this difficulty include: (i) The dynamic interaction between the picking roller and the stalk involves intricate motion processes, rendering the precise tracking of motion trajectories difficult (T. Y. Li et al., 2023; Zhang et al., 2023). (ii) Maize stalks are composed of multiple materials, such as cellulose and lignin, exhibiting anisotropic characteristics. Their deformation under external forces is complex and difficult to express using conventional mathematical models (Oduntan et al., 2024). (iii) The contact area between the stalk and the picking roller is limited, making it impossible to observe the effect of the picking roller's surface structure on the stalk at a microscopic level (Luo et al.,

2023). Previous studies on ear-picking devices have primarily focused on developing numerical models and conducting bench tests (Fu et al., 2023; T. Y. Li et al., 2023), but they lack microscopic investigations into the interaction between the picking roller surface structure and the stalk. To address these limitations, this study employs a DEM-MBD coupled simulation approach to analyse the effect of the picking roller surface structure on the stalk. This method enables accurate simulation of the dynamic interaction and deformation behavior of maize stalks under realistic operating conditions, visualises the stalk-pulling process, and thus provides deeper insight into the mechanisms affecting stalk pulling force. Currently, the DEM-MBD coupled simulation method has been validated as an effective simulation tool for investigating the influence of mechanical motion on granular interactions (Fang et al., 2024; He et al., 2025; Xie et al., 2024).

In the field of agricultural machinery research, discrete element stalk models have been widely employed to study the interactions among agricultural machinery, stalks, and soil, as well as the mechanical properties of stalks themselves (Jin et al., 2024; Lin et al., 2024; L. Liu, Wang, Zhang, Cheng, et al., 2023). Most existing stalk models employ single-layer flexible homogeneous structures, which fail to accurately represent the internal structural differences and fracture mechanisms of real maize stalks. Therefore, this study constructs an interaction model between a vibration-enabled ear-picking device and the stalk based on a dual-layer particle-based flexible stalk model, aiming to explore the interaction between the picking mechanism and the maize stalk. The model uses particles with different parameters to represent the distinct mechanical properties of the stalk epidermis and core, enabling accurate simulation of elastic deformation and fracture behavior under dynamic tensile loading. This approach provides a more realistic representation of the mechanical response of maize stalks during the ear-picking process and improves the accuracy of the simulation results. At present, research on the interactions between picking devices and maize stalks remains limited. Existing studies on stalk-roller interactions have mainly focused on roller design and macroscopic parameter regulation, such as roller speed, roller clearance, and feeding angle (Y. Li et al., 2016; Qin et al., 2020). However, these studies have not provided an in-depth understanding of the microscopic contact mechanisms associated with roller surface structures, nor have they systematically analysed how these microscopic processes influence stalk pulling force and its variation. Therefore, knowledge of how to optimise roller surface structures to enhance pulling force and improve picking performance remains insufficient.

The objectives of this study are as follows: (i) To establish a picking roller-stalk interaction model using a dual-layer flexible stalk model. (ii) To validate the accuracy of the model through bench tests and simulation experiments. (iii) To investigate the influence of picking roller surface structures on stalk pulling force using the developed interaction model.

2. Materials and methods

2.1. Overall Structure and Working Principle

The vibration ear-picking cutting table primarily consists of a crop divider, cutting knife, convey chain, pressing rod, ear-picking device, and ear conveying device, as shown in Fig. 1a. Among them, the ear-picking device is the core component of the vibration cutting table, primarily consisting of picking rollers, chain wheel, and stalk pulling rollers, as shown in Fig. 1b. The picking rollers adopt a polyhedral configuration with unequal interior angles and are configured in a large-angle-to-small-angle arrangement. When a maize stalk is fed into the gap between the picking rollers, it undergoes high-frequency vibration in both left and right directions under the influence of the picking roller's external structure, a phenomenon referred to as excitation (Fig. 1c) (Geng et al., 2019). During the ear picking process, as the clamping position moves closer to the ear formation position, the excitation force

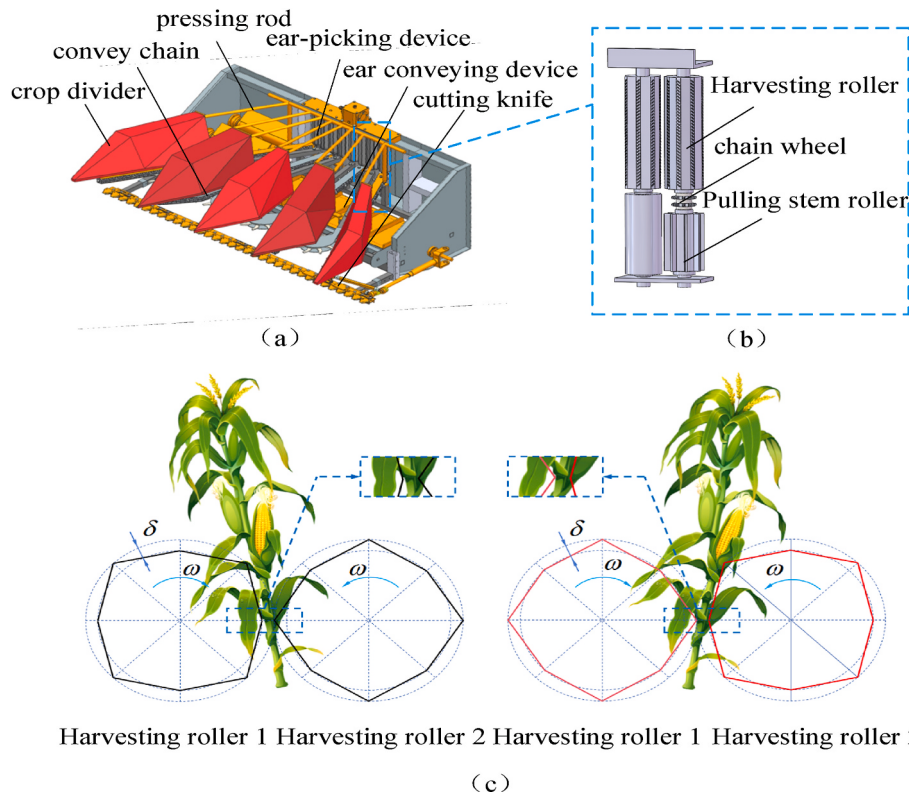


Fig. 1. Structure and Working Principle of the Vibration Ear-Picking Cutting Table (a) Vibration Ear-Picking Cutting Table (b) Ear-Picking Device (c) External Structure and Working Principle of the Ear Picking Rollers Note: δ represents the amplitude of the ear picking rollers.

exerted on the ear gradually intensifies. Once the excitation force surpasses the connection strength between the ear and the ear shank or between the ear shank and the stalk, the ear is detached. Since achieving stable clamping and effective vibration transmission requires reliable stalk gripping without causing stalk breakage, enhancing the gripping reliability of the picking rollers has become the critical focus of this study.

2.2. Measurement of stalk compression properties

Vibration ear picking refers to applying high-frequency vibrations to the stalk during clamping and conveying to achieve ear-stalk separation. Evidently, a smaller gap between the picking rollers improves the reliability of stalk clamping and increases the clamping force. However, if the gap is excessively small, not only does stalk feeding become difficult, but it also leads to stalk breakage, resulting in vibration ear picking cutting table clogging and operational disruptions. Conversely, a larger gap facilitates smooth stalk feeding and prevents stalk breakage, but insufficient clamping force weakens the transmission of excitation forces, potentially leading to ineffective ear detachment. To enhance the clamping force of the picking rollers on the stalk and reduce the occurrence of stalk breakage, a stalk compression resistance test was conducted. Maize stalk samples were collected from a maize experimental field in Jiangmiao Village, Huantai County, Zibo City, Shandong Province. The maize stalk samples were strictly selected to ensure no visible damage or disease. The fourth internode from the root was chosen as the reference point, and stalk segments with a length of 20 mm (excluding internodes) were precisely cut using a sharp blade. Before testing, each stalk segment was measured five times in different directions using a digital vernier caliper (accuracy ± 0.01 mm) to ensure that the average diameter was 24 ± 2 mm. During the compression test, each prepared stalk sample was placed horizontally on the platform of the universal testing machine (WDW-5M electronic universal testing

machine). A circular rigid compression plate was securely mounted on the movable beam of the testing machine and aligned vertically above the stalk sample to ensure full and uniform contact during compression. Prior to testing, the beam was manually lowered slowly until the digital controller of the machine indicated a slight initial preload of approximately 1 N, ensuring consistency in the initial gap. The formal compression test was then initiated, applying vertical compression to the stalk sample at a constant rate of 3 mm/s, continuing until significant structural failure of the stalk occurred.

2.3. DEM-MBD coupled model

2.3.1. Contact model

The contact model in this study includes the Hertz-Mindlin (no slip) model and the Hertz-Mindlin with Bonding V2 model. The Hertz-Mindlin (no slip) model (Fig. 2a) is used for contact analysis between the stalk and the smooth surfaces of the ear-picking device. This model decomposes the contact force into a normal force with a damping component and a tangential force. The Hertz-Mindlin with Bonding V2 contact model (Fig. 2b) is used to describe the flexible characteristics of the stalk. The governing Eqs. for the Hertz-Mindlin (no slip) contact model are as follows (Tang et al., 2023).

The normal force is calculated using the following Eq. (1):

$$F_n = \frac{4}{3}E^* \sqrt{R^*} \delta_n^{\frac{3}{2}} \quad (1)$$

Where E^* is the equivalent Young's modulus (Pa); R^* is the equivalent radius (m); δ_n is the normal overlap between particles (m).

$$\frac{1}{E^*} = \frac{(1 - \nu_1^2)}{E_1} + \frac{(1 - \nu_2^2)}{E_2} \quad (2)$$

$$\frac{1}{R^*} = \frac{1}{R_1} + \frac{1}{R_2} \quad (3)$$

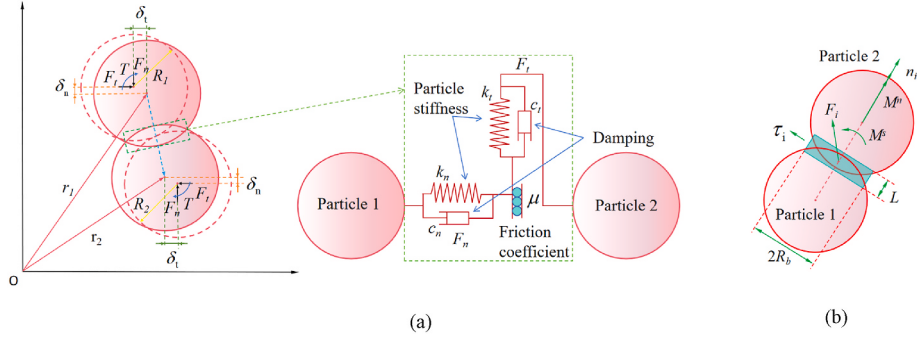


Fig. 2. Contact Model (a) Hertz-Mindlin (no slip) Contact Model (b) Hertz-Mindlin with Bonding V2 contact model.

$$\delta_n = R_1 + R_2 - |\mathbf{r}_1 - \mathbf{r}_2| \quad (4)$$

where ν_1 and ν_2 are the Poisson's ratios of particle 1 and particle 2, respectively; E_1 and E_2 are the Young's modulus of particle 1 and particle 2 (Pa), respectively; R_1 and R_2 are the radius of particle 1 and particle 2 (m), respectively; \mathbf{r}_1 and \mathbf{r}_2 are the position vectors of the centers of particle 1 and particle 2, respectively.

The normal damping force is calculated using the following Eq. (5):

$$F_n^d = -2\sqrt{\frac{5}{6}}\beta\sqrt{S_n m^*} v_n \vec{vel} \quad (5)$$

Where F_n^d is the normal damping force (N); β is the coefficient related to the restitution coefficient; S_n is the normal stiffness ($N \cdot m^{-1}$); m^* is the equivalent mass (g); $v_n \vec{vel}$ is the normal component of the relative velocity ($m \cdot s^{-1}$).

$$m^* = \left(\frac{1}{m^1} + \frac{1}{m^2} \right)^{-1} \quad (6)$$

$$\beta = \frac{-\ln e}{\sqrt{\ln^2 e + \pi^2}} \quad (7)$$

$$S_n = 2E^* \sqrt{R^* \delta_n} \quad (8)$$

Where e is the coefficient of restitution.

The tangential force is calculated using the following Eq. (9):

$$F_t = -S_t \delta_t \quad (9)$$

Where F_t is the tangential force between particles (N); S_t is the tangential stiffness ($N \cdot m^{-1}$); δ_t is the overlap coefficient (m).

$$S_t = 8G^* \sqrt{R^* \delta_t} \quad (10)$$

Where G^* is the equivalent shear modulus (Pa).

$$G^* = \frac{(2 - \nu_1^2)}{G_1} + \frac{(2 - \nu_2^2)}{G_2} \quad (11)$$

Where G_1 and G_2 are the shear modulus of particle 1 and particle 2 (Pa), respectively.

The tangential damping force between particles is calculated using the following Eq. (12):

$$F_t^d = -2\sqrt{\frac{5}{6}}\beta\sqrt{S_t m^*} v_t \vec{vel} \quad (12)$$

Where F_t^d is the tangential damping force (N); $v_t \vec{vel}$ is the tangential component of the relative velocity ($m \cdot s^{-1}$).

The Hertz-Mindlin with Bonding V2 contact model bonds particles together using parallel bonds, forming elastic bonding elements. These bonds are distributed at particle contact points and are represented by

forces and moments. Once the bonds are established, the forces and moments are reset to zero and subsequently updated at each time step according to Eqs. 13–18 through an iterative process (Shi et al., 2023).

$$\delta F_n = -\nu_n S_n A \delta z \quad (13)$$

$$\delta F_t = -\nu_t S_t A \delta z \quad (14)$$

$$\delta M_n = -\omega_n S_t J \delta z \quad (15)$$

$$\delta M_t = -\omega_t S_n \frac{J}{2} \delta z \quad (16)$$

Where δF_n and δF_t are the normal bonding force and tangential bonding force (N), respectively; δM_n and δM_t are the normal moment and tangential moment (N·m), respectively; ν_n and ν_t are the normal velocity and tangential velocity ($m \cdot s^{-1}$), respectively; ω_n and ω_t are the normal angular velocity and tangential angular velocity ($rad \cdot s^{-1}$), respectively; S_n and S_t are the normal stiffness and tangential stiffness, respectively; A is the particle contact area; J is the moment of inertia; δz is the time step.

$$A = \pi R_b^2 \quad (17)$$

$$J = \frac{1}{2} \pi R_b^4 \quad (18)$$

The fracture of the bonding bond is determined based on Eqs. 19 and 20.

$$\sigma_{max} < \frac{-F_n}{A} + \frac{2M_n R_b}{J} \quad (19)$$

$$\tau_{max} < \frac{-F_t}{A} + \frac{M_n R_b}{J} \quad (20)$$

Where R_b is the bonding radius; σ_{max} and τ_{max} are the normal critical stress and tangential critical stress, respectively.

2.3.2. DEM model

To accurately construct a flexible stalk model, a dual-layer stalk model was developed using the discrete element software EDEM 2021.2. Given that the objective of this study is to enhance the stalk pulling force of the picking rollers to facilitate ear-stalk separation, only the stalk section below the ear formation position and above stalk cutting position was modeled. The stalk length is 550 mm, the stalk diameter is 24 mm, and the epidermis thickness is 2 mm. Two types of particles with different parameters were used to fill the stalk epidermis and the stalk core, with a particle size of 1 mm and a contact radius of 1.2 mm. The Poisson's ratio, shear modulus, and density of the stalk epidermis, the stalk core, and steel were referenced from relevant literature (M. Chen et al., 2024; Y. Liu et al., 2022). The contact parameters between the stalk epidermis, the stalk core, and ear-picking device, as well as the bonding parameters between the epidermis and the core, were determined based on (Liu et al., 2023; Xiao et al., 2022). The simulation

parameters are shown in Tables 1–3, and the generated stalk model is shown in Fig. 3.

2.3.3. MBD model

The vibration ear picking cutting table consists of numerous parts. If all these parts are placed into RecurDyn 2023 for simulation, it would significantly increase computational load and reduce simulation efficiency. Therefore, in alignment with the objective of this study, only the picking device was modeled, as shown in Fig. 4a. During actual operation, before entering the gap between the picking rollers, the maize stalk is guided by a pressing rod, ensuring a feeding angle of 40°–50°. In this study, a fixed feeding angle of 45° was used.

To investigate the influence of picking roller surface structures on stalk pulling force during the ear-picking process, three different surface structures were constructed.

- (i) The surface is designed with symmetrically inclined pattern structures (Fig. 4b), where the inclined patterns form a 45° angle with the axis of the picking roller.
- (ii) The surface is designed with interlaced pattern structures (Fig. 4c), where the interlacing angle is 90°, and the inclination angle relative to the picking roller axis is 45°.
- (iii) The surface is designed with arc-shaped pattern structures (Fig. 4d), where the tangent at the center of the arc forms a 45° angle with the picking roller axis, and the arc radius R is 240 mm.

2.3.4. Coupled simulation model

Using the parameters of the stalk epidermis and the stalk core obtained in Section 2.3.2, a maize stalk model was constructed with a diameter of 24 mm, a length of 550 mm, and an epidermis thickness of 2 mm. The modelling method is as follows:

First, the gravity direction was set to the -Z axis. A cylinder with a diameter of 24.3 mm and a length of 550 mm, and another cylinder with a diameter of 20 mm and a length of 550 mm were created. The outer cylinder with a diameter of 24.3 mm and length of 550 mm was used as a container for generating epidermis particles, while the inner cylinder with a diameter of 20 mm was used to define the core region. The diameter of the outer cylinder was intentionally set slightly larger than the actual stalk diameter (24 mm) to allow for sufficient particle filling and compaction. After particle generation and stabilization, the outer cylinder was adjusted to 24 mm to match the target geometry of the maize stalk, ensuring dense and uniform particle packing prior to bonding. A total of 6007 epidermis particles and 10,111 core particles were generated, along with 14,986 epidermis particle bonds and 41,832 core particle bonds.

The ear-picking device model was created using SolidWorks 2022. Based on actual structural dimensions, the model-including the picking rollers, chain wheel, and stalk-pulling rollers-was constructed in SolidWorks and then exported in STEP format. The model was imported into RecurDyn 2023 using the “Import” function. After import, the “Merge” command in RecurDyn was used to combine the picking rollers, chain wheel, and stalk-pulling rollers into a single assembly. Rotational constraints were applied, and a driving force was assigned to provide power

Table 1
Intrinsic parameters.

Material	Parameters	Value
Stalk epidermis	Poisson's ratio	0.3
	Shear modulus (Pa)	3.87×10^8
Stalk core	Density ($\text{kg}\cdot\text{m}^{-3}$)	1570
	Poisson's ratio	0.4
Steel	Shear modulus (Pa)	8.13×10^6
	Density ($\text{kg}\cdot\text{m}^{-3}$)	1060
	Poisson's ratio	0.25
Shear modulus (Pa)		7.9×10^{10}
Density ($\text{kg}\cdot\text{m}^{-3}$)		7850

Table 2
Contact parameters.

Material	Parameters	Value
Stalk epidermis-Stalk epidermis	Restitution coefficient	0.485
	Static friction coefficient	0.142
Stalk epidermis-Stalk core	Dynamic friction coefficient	0.078
	Restitution coefficient	0.263
Stalk core-Stalk core	Static friction coefficient	0.495
	Dynamic friction coefficient	0.166
Steel-Stalk epidermis	Restitution coefficient	0.348
	Static friction coefficient	0.427
Steel-Stalk core	Dynamic friction coefficient	0.144
	Restitution coefficient	0.663
Steel-Stalk core	Static friction coefficient	0.23
	Dynamic friction coefficient	0.13
Steel-Stalk core	Restitution coefficient	0.325
	Static friction coefficient	0.38
	Dynamic friction coefficient	0.15

Table 3
Contact model parameters.

Material	Parameters	Value
Stalk epidermis	Normal stiffness ($\text{N}\cdot\text{m}^{-2}$)	9.689×10^8
	Tangential stiffness ($\text{N}\cdot\text{m}^{-2}$)	5.002×10^8
	Critical normal stress (Pa)	4.97×10^{12}
	Critical tangential stress (Pa)	3.097×10^{12}
Stalk core	Normal stiffness ($\text{N}\cdot\text{m}^{-2}$)	2.04×10^9
	Tangential stiffness ($\text{N}\cdot\text{m}^{-2}$)	1×10^9
	Critical normal stress (Pa)	1.705×10^{12}
	Critical tangential stress (Pa)	1.03×10^{12}

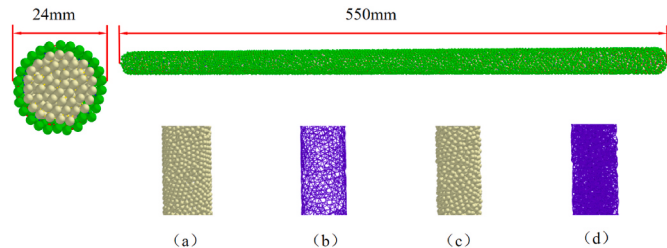


Fig. 3. Stalk model (a) Stalk epidermis model (b) Stalk epidermis particle bonding (c) Stalk core model (d) Stalk core particle bonding.

to the picking rollers. The remaining components were fixed to the ground using fixed constraints. Through the External SPI module, a Wall file was generated and imported into EDEM software. In EDEM, the direction cosine matrix was applied to adjust the feeding angle of the maize stalk, followed by the generation of the stalk model, ultimately completing the establishment of the coupled simulation model, as shown in Fig. 5.

2.4. Bench validation of the DEM-MBD coupled model

2.4.1. Measurement of performance indicators in actual tests

(1) Measurement of the Maximum Stalk Pulling Force of the Picking Rollers

The experiment was conducted in the Agricultural Machinery Equipment Laboratory at Shandong University of Technology. The stalk pulling force measurement test was performed on a vibration ear-picking test bench, as shown in Fig. 6. The test bench primarily consists of a motor (Model: YE2-100L-2, Speed Range: 0–2870 $\text{r}\cdot\text{min}^{-1}$), a torque sensor (Model: HCNJ-101, Torque Range: 0–100 N m, Speed Range: 0–1000 $\text{r}\cdot\text{min}^{-1}$), a frequency converter, cutting knife, convey

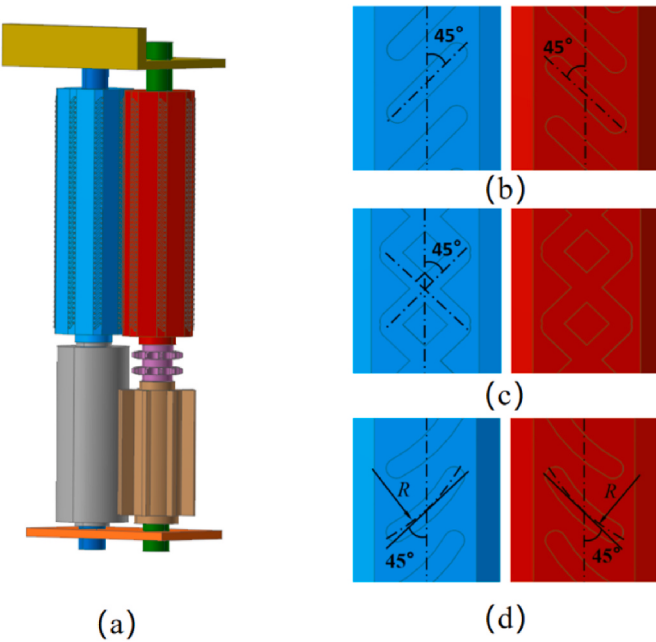


Fig. 4. MBD model (a) Ear-picking device Model (b) Inclined pattern structures (c) Interlaced pattern structures (d) Arc-shaped pattern structures.

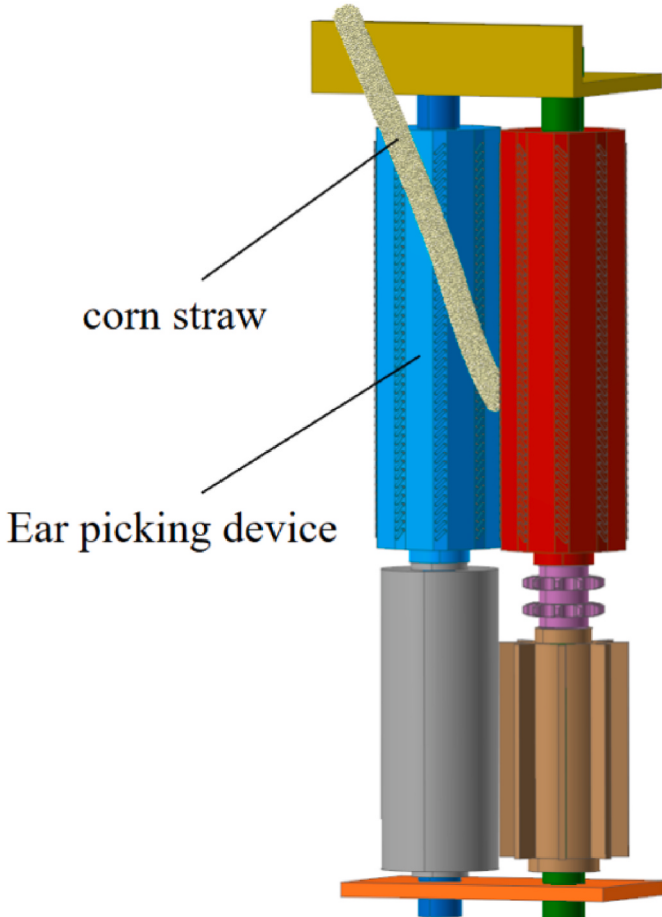


Fig. 5. Coupled simulation model.

chain, a pressing plate, and a ear-picking device. The motor is connected to the picking rollers via the torque sensor, providing the necessary power for the picking rollers while simultaneously driving the convey chain. The torque sensor records the torque variations during the stalk-pulling process. To simulate the natural growth state of maize in the soil, maize stalks were fixed onto an aluminum frame using clamps. The rotational speed of the picking rollers was set to 950 r·min⁻¹ based on previous research (Geng et al., 2019). To prevent experimental interference caused by stalk breakage, the picking gap was set to 12 mm. The surface structure of the picking rollers featured inclined patterns, with a pattern width of 2 mm, pattern length of 8 mm, pattern height of 1 mm, and pattern spacing of 8 mm for the bench test. At the conclusion of the experiment, torque sensor data were recorded, and the maximum stalk pulling force of the picking rollers was calculated using Eq. (21). To ensure the experiment was conducted at a stable rotational speed, a preliminary idle run was included before testing, allowing the picking rollers to reach steady-state operation.

$$F_{max} = \frac{T_{max}}{d} \quad (21)$$

Where F_{max} is the maximum stalk pulling force (N); T_{max} is the maximum torque (N·m); d is the average radius of the picking roller (m).

(2) Measurement of Power Consumption of the Ear-Picking Device

During the ear-picking experiment, the torque sensor installed on the test bench was used to continuously monitor the torque in real time throughout the ear-picking process. The real-time torque values were exported using the M400 software associated with the torque sensor and subsequently plotted using Origin 2024 software. The integration module in Origin was then employed to integrate the torque curve before the ear detachment, and the power consumption was obtained using Eq. (22).

$$W = \frac{\pi n \int_0^t T dt}{30} \quad (22)$$

Where W is the power consumption (W); n is the rotational speed of the picking roller (r·min⁻¹); T is the real-time torque of the picking roller (N·m).

2.4.2. Measurement of performance indicators in simulation tests

(1) Measurement of the Maximum Stalk Pulling Force of the Ear Picking Rollers

Referring to Sections 2.3.3, a ear-picking device model consisting of picking rollers with inclined pattern structures (with pattern parameters identical to those used in the actual experiment) was established using SolidWorks 3D modelling software. The model was then imported into RecurDyn, where the constraints described in Section 2.3.4 were applied, and the picking roller speed was set to 950 r·min⁻¹. Finally, a Wall file was generated and imported into EDEM software, where the maize stalk model was created, and the simulation experiment was conducted. Upon completion of the simulation, the post-processing module in EDEM was used to analyse the contact interactions between the picking rollers and the maize stalk and to obtain the variation curve of stalk pulling force over time. Subsequently, the maximum stalk pulling force of the picking rollers was determined using the EDEM post-processing module.

(2) Measurement of Power Consumption of the Ear Picking Device

Through the EDEM post-processing module, the real-time torque during the stalk pulling process was obtained. Using the same method as in the actual experiment, the real-time torque data was fitted in Origin

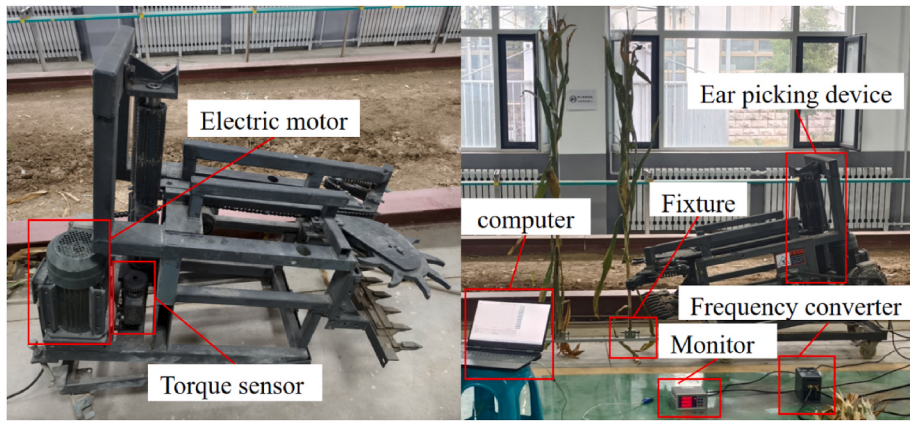


Fig. 6. Experimental setup for stalk pulling force test.

software and then integrated using the integration module. Finally, the power consumption of the ear picking device was determined using Eq. (22).

2.4.3. Model validation and application

To verify the accuracy of the established coupled simulation model, a validation test was conducted by comparing its results with those from the physical bench tests. Both the simulation experiment and the actual experiment utilized picking rollers with inclined patterns featuring identical parameters, with the picking roller speed set to $950 \text{ r} \cdot \text{min}^{-1}$. The maximum stalk pulling force and power consumption values obtained from the simulation experiment were compared with the actual test values, and the relative error was used to evaluate the accuracy of the model. The relative error was used to evaluate the accuracy of the model. To avoid experimental contingency, five sets of tests were conducted for both the simulation experiment and the actual experiment.

Due to the difficulty in obtaining experimental data in bench tests, the validated simulation model was used to study the influence of picking roller surface structures on stalk pulling force. The pattern shape, pattern height, and pattern spacing of the picking rollers were selected as experimental factors. The pattern shapes considered were inclined patterns, interlaced patterns, and arc-shaped patterns. Regarding pattern height, excessively high patterns enhance the gripping force on the stalk but also increase stalk damage, making stalk breakage more likely. Conversely, excessively low patterns may fail to effectively grip the stalk, potentially reducing ear picking efficiency. Based on relevant research (Rossi & McGuire, 1992; F. Yang, Chen, et al., 2021), the pattern heights were set at 1 mm, 1.5 mm, 2 mm, 2.5 mm, and 3 mm. Pattern spacing affects gripping uniformity and the stability of stalk pulling force. A smaller spacing allows for more uniform gripping, enhancing the stability of overall stalk pulling force, while a larger spacing reduces the effective contact area, leading to insufficient gripping force (Opheim, 1994). The pattern spacing was set at 5 mm, 6.5 mm, 8 mm, 9.5 mm, and 11 mm.

2.5. Data analysis

Data analysis was conducted using IBM SPSS Statistics 26. Duncan's multiple range test was employed for significance analysis, with a significance level set at 0.05. With pattern spacing fixed, a main effect and interaction effect analysis was performed on pattern shape and pattern height to determine the optimal pattern height. With pattern height fixed, a main effect and interaction effect analysis was conducted on pattern shape and pattern spacing.

3. Results

3.1. Mechanical properties test results of maize stalks

During the stalk compression force test, the computer collected load and displacement data points and plotted them as a compression force variation curve, as shown in Fig. 7. The maximum compression force that the maize stalk can withstand was determined by averaging the results from multiple compression force tests, as shown in Table 4.

In the initial stage of the stalk compression test (0–2 s), the compression force exhibited a slow increasing trend due to the compressibility of the stalk core. In the second stage (2–3.5 s), the stalk core material became compacted, resulting in a rapid increase in compression force. In the third stage (3.5–5 s), the stalk material reached its maximum compressive strength, resulting in stalk compression damage. In the fourth stage (5–7.1 s), the entire maize stalk became fully compacted, causing a compression increase in the measured force, which marked the completion of the test.

3.2. Validation results of bench tests and simulation experiments

The maximum stalk pulling force and power consumption values measured through simulation and bench tests under identical conditions are shown in Fig. 8. From the results of both the simulation and bench

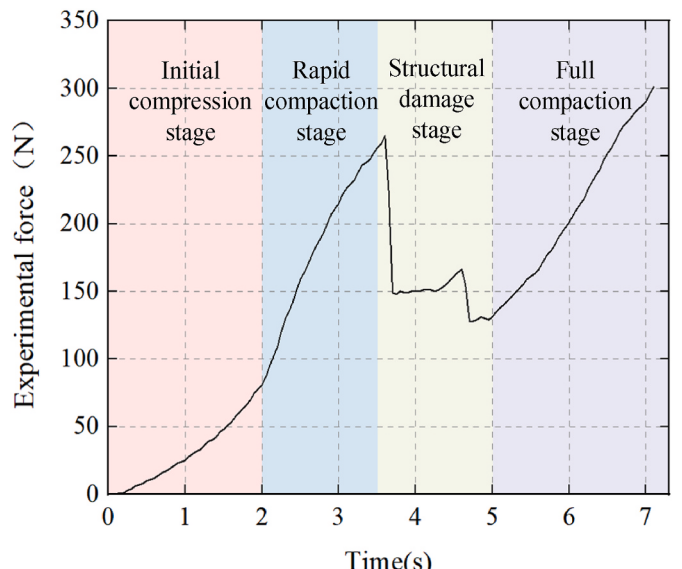


Fig. 7. Compression test results.

Table 4
Maize stalk compression test results.

Materials	The maximum scale compression (N)		Average maximum compression force (N)
	Max	Min	
Maize stalk	272.54	246.63	260.13

tests, the average maximum stalk pulling force (Fig. 8a) was 48.040 N in the simulation and 50.800 N in the bench test, with a relative error of 5.400 %. Similarly, the average power consumption (Fig. 8b) was 53.528 W in the simulation and 56.454 W in the bench test, corresponding to a relative error of 5.183 %. The causes of the error are mainly attributed to two factors. The stalk model used in the simulation was simplified as a uniform-diameter structure, while in reality, the internode diameter of actual maize stalks varies along the stalk, leading to changes in the contact area and frictional behavior during stalk pulling, which may affect the peak stalk pulling force. In addition, the feeding angle in the simulation was fixed at 45°, whereas in bench tests, slight deviations in stalk positioning are inevitable. These variations influence the interaction posture and the effective friction engagement between the stalk and the picking roller, thereby impacting the measured stalk pulling force. Overall, the simulation results closely approximate the measurements from the bench tests, demonstrating that the established DEM-MBD coupled simulation model can effectively simulate the stalk-pulling process of an actual ear-picking device.

3.3. Dynamic simulation of three surface structures under different structural parameters

Table 5 presents the maximum stalk pulling force test values and their error ranges, obtained from multiple trials conducted at a fixed pattern spacing of 8 mm while varying pattern shapes and heights. Here, A1, A2, and A3 represent inclined patterns, interlaced patterns, and arc-shaped patterns, respectively, while B1, B2, B3, B4, and B5 correspond to different pattern heights.

The variation in stalk pulling force corresponding to different pattern heights for picking rollers with three pattern shapes is shown in Fig. 9. It can be observed that with the increase in pattern height, the stalk pulling force increases across all three pattern types. This trend is attributed to mechanical changes at the contact interface. As the pattern height increases, the contact area and embedding depth between the roller surface and the maize stalk also increase. This enhances the normal clamping force and tangential frictional force exerted by the picking roller on the stalk, allowing the roller to grip the stalk more firmly during rotation. Additionally, higher patterns are more likely to partially embed into the stalk epidermis, improving mechanical engagement and reducing slippage. During the stalk pulling process, the stalk enters the picking gap and interacts with the surface patterns of the picking rollers.

The roller surface patterns first break the bonding between the epidermal particles of the stalk and then gradually embed into the inner tissues, exerting a gripping effect on the internal particles. Differences in pattern height lead to variations in embedding depth, which in turn result in different levels of force applied to the internal particles of the stalk, as illustrated in Fig. 10. The variation in stalk pulling force observed among different pattern shapes at the same pattern height is caused by differences in contact geometry, friction directionality, and mechanical interlocking behavior at the roller-stalk interface. Different pattern shapes result in distinct modes of interaction with the stalk

Table 5
Stalk pulling force under the influence of pattern shape A and pattern height B.

Pattern height B	Stalk pulling force(N)		
	A1	A2	A3
B1	48.125 ± 0.427 a	52.250 ± 0.420 a	47.650 ± 0.387 a
	A	B	A
B2	58.050 ± 0.465 b	65.200 ± 0.529 b	60.075 ± 0.499 b
	A	C	B
B3	62.225 ± 0.411 c	66.350 ± 0.443 c	63.350 ± 0.379 c B
	A	C	B
B4	74.250 ± 0.520 d	73.275 ± 0.403 d	66.675 ± 0.479 d
	C	B	A
B5	78.825 ± 0.435 e	81.150 ± 0.451 e	78.875 ± 0.435 e
	A	B	A

Note: Different lowercase letters in the table indicate significant differences ($p < 0.05$) in stalk pulling force among different pattern heights B at the same pattern shape A level. Different uppercase letters in the figure indicate significant differences ($p < 0.05$) in stalk pulling force among different pattern shapes A at the same pattern height B level.

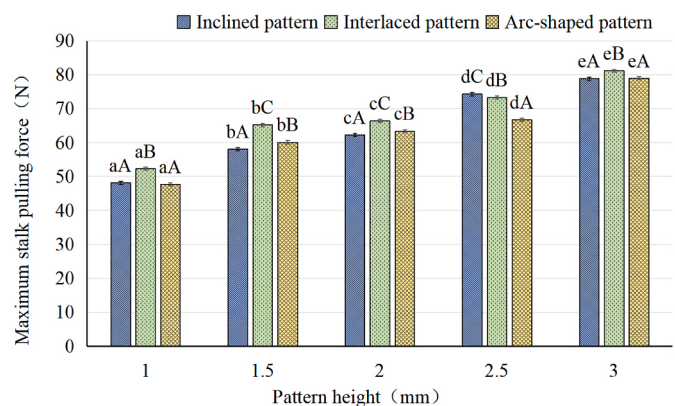


Fig. 9. Comparison of maximum stalk pulling force under the influence of pattern shape A and pattern height B.

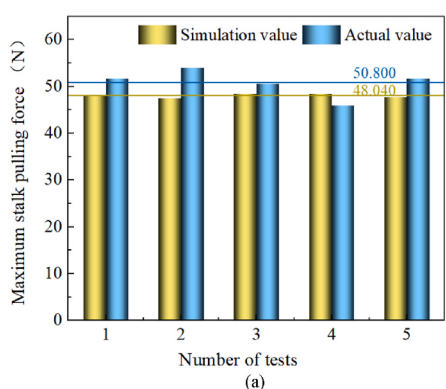
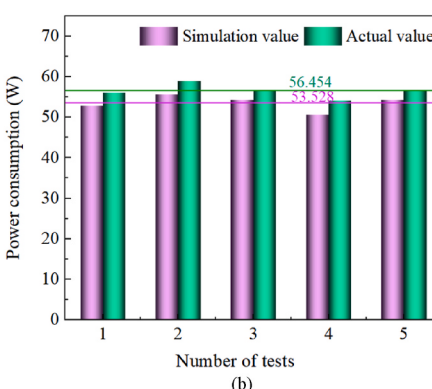


Fig. 8. Bench test validation results (a) Maximum stalk pulling force validation results (b) Power consumption validation results.



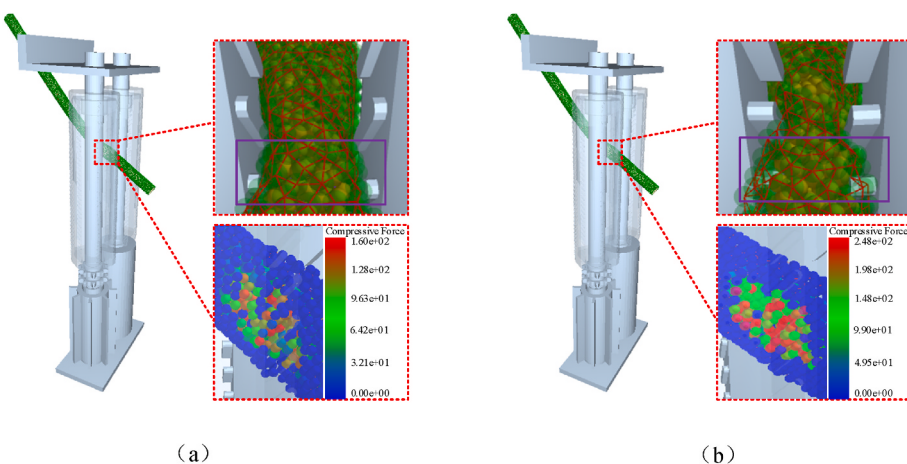


Fig. 10. Contact states between the stalk and different pattern heights at the same spacing (a) contact state with a pattern height of 1 mm (b) contact state with a pattern height of 2.5 mm.

surface. For example, inclined patterns provide a directional friction path aligned with the stalk's axial direction, enabling a smoother and more continuous pulling effect. In contrast, interlaced patterns create alternating friction vectors due to their crisscross structure, which can increase the instantaneous gripping force but may also introduce fluctuations in traction. Arc-shaped patterns, with their smooth curved geometry, often produce stronger localised engagement due to concentrated contact pressure.

Severely compressed maize stalks are prone to breakage when pulled by the picking rollers (Fig. 11), leading to ear picking cutting table clogging and reducing ear-picking efficiency. The relationship between the stalk pulling force applied by the picking rollers and the compression

force can be described by Eq. (23), where the friction coefficient between the picking rollers and the maize stalk ranges from $f = 0.3\text{--}0.6$ (G. Chen, Liu, et al., 2024; Z. Y. Li et al., 2024). Based on the mechanical properties of maize stalks measured in Section 3.1, the critical stalk pulling force required to prevent stalk breakage is calculated to be 78,039 N.

$$F_1 = \mu \times F_2 \quad (23)$$

Where F_1 represents the stalk pulling force (N); F_2 represents the compression force (N); μ represents the friction coefficient.

When the pattern height is 3 mm, the maximum stalk pulling forces generated by picking rollers with inclined, interlaced, and arc-shaped patterns are 78.825 N, 81.150 N, and 78.875 N, respectively. Under this conditions, the picking rollers may cause stalk breakage during pulling. When the pattern height is 2.5 mm, the maximum stalk pulling forces generated by picking rollers with inclined, interlaced, and arc-shaped patterns are 74.250 N, 73.275 N, and 66.675 N, respectively. At this time, no stalk breakage occurs during operation. Therefore, a pattern height of 2.5 mm was selected for further investigation of the influence of pattern shape and pattern spacing on stalk pulling force.

At a pattern height of 2.5 mm, the stalk pulling force test values and their error ranges obtained from multiple trials with different pattern shapes and pattern spacings are shown in [Table 6](#). Here, A1, A2, and A3 represent inclined patterns, interlaced patterns, and arc-shaped patterns, respectively, while B1, B2, B3, B4, and B5 correspond to different pattern spacings.

Table 6
Stalk pulling force under the influence of pattern shape A and pattern spacing C.

Pattern Spacing C	Stalk pulling force(N)		
	A1	A2	A3
C1	94.050 ± 0.532 e B	133.15 ± 0.624 e C	88.600 ± 0.424 e A
C2	72.300 ± 0.424 c C	61.725 ± 0.479 a A	70.625 ± 0.465 d B
C3	74.250 ± 0.52 d C	73.275 ± 0.403 b B	66.675 ± 0.479 b A
C4	70.325 ± 0.479 b B	81.625 ± 0.403 c C	69.175 ± 0.585 c A
C5	66.750 ± 0.48 a B	85.900 ± 0.648 d C	62.975 ± 0.457 a A

Note: Different lowercase letters in the table indicate significant differences ($p < 0.05$) in stalk pulling force among different pattern spacings C at the same pattern shape A level. Different uppercase letters in the figure indicate significant differences ($p < 0.05$) in stalk pulling force among different pattern shapes A at the same pattern spacing C level.

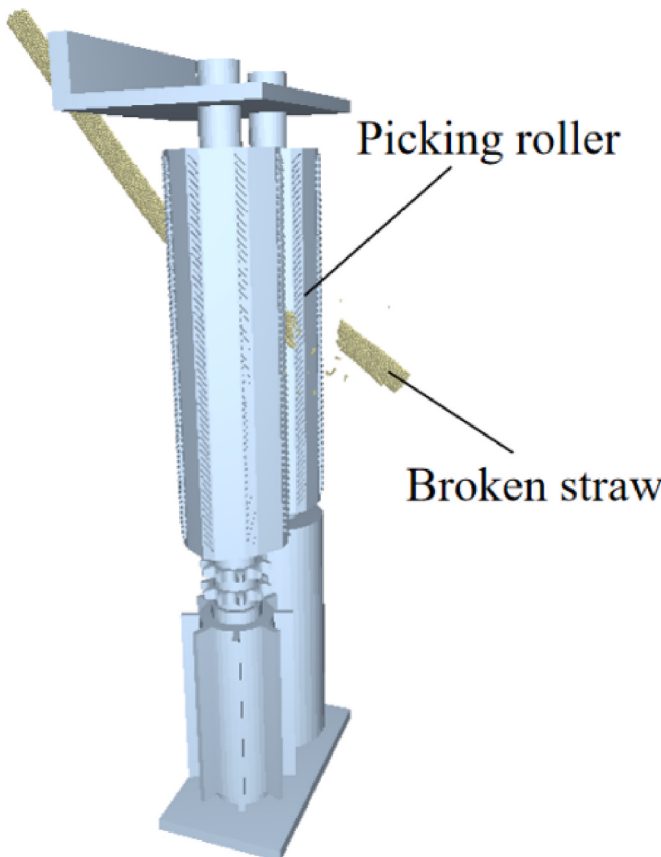


Fig. 11. Stalk breakage caused by picking rollers.

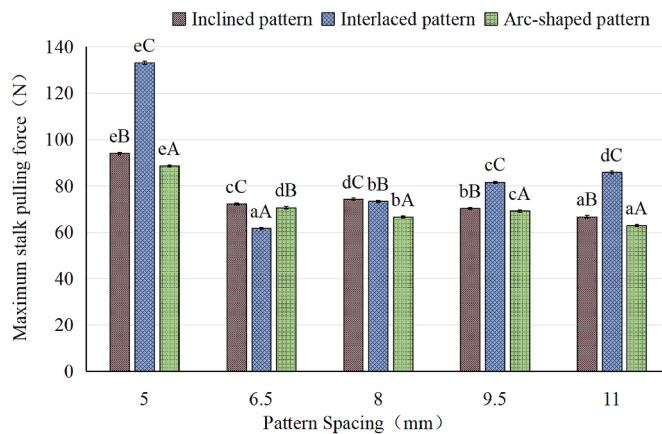


Fig. 12. Comparison of maximum stalk pulling force under the influence of pattern shape A and pattern spacing C.

The variation in maximum stalk pulling force corresponding to different pattern spacings for picking rollers with various pattern shapes is shown in Fig. 12. As the pattern spacing increases, the maximum stalk pulling forces of the inclined and arc-shaped patterns show a trend of first decreasing and then stabilising. This indicates that their effective contact area with the stalk gradually decreases as the spacing increases; however, once the spacing exceeds a certain threshold, the contact area becomes stable, and consequently, the pulling force remains nearly constant. In contrast, the interlaced pattern exhibits a variation trend of first sharply decreasing and then gradually increasing. At smaller spacings, the interlaced pattern can form a larger effective contact area and multidirectional frictional forces. In this case, the effect of the patterns on the stalk is not primarily achieved by deeply embedding into the internal particles to enhance gripping capacity, but rather by excessively breaking the bonding between stalk particles, leading to local compaction. This excessive clamping increases the pulling force, resulting in extremely high values (Fig. 13a). As the spacing increases, the gaps between the patterns gradually widen, and the originally dense and continuous contact points decrease, causing insufficient contact coverage between the roller surface and the stalk. At this stage, the rollers no longer impose excessive clamping on the stalk, and the patterns are also unable to embed deeply into the internal particles to achieve effective gripping, thereby causing a significant reduction in pulling force (Fig. 13b). When the spacing increases further, the patterns can once again embed into the stalk interior and interact with the internal particles, forming new force-bearing points and thus increasing the pulling force (Fig. 13c). When the pattern spacing was 5 mm, the maximum stalk pulling forces of the three pattern structures all reached

their peak values, with the interlaced pattern being the highest at 133.150 N, followed by the inclined and arc-shaped patterns at 94.050 N and 88.600 N, respectively. These pulling forces clearly exceeded the critical stalk pulling force of 78.039 N, which could easily cause severe stalk breakage. Therefore, the three configurations with a 5 mm spacing, as well as other parameter combinations that resulted in pulling forces exceeding the critical threshold, are not practically applicable in the optimisation process and should be excluded from the optimal scheme.

The analysis of variance ANOVA for the effects of pattern shape and pattern height on stalk pulling force is shown in Table 7. It can be observed that pattern shape, pattern height, and their interaction have a highly significant effect on stalk pulling force ($p < 0.01$). As pattern height increases, the stalk pulling force for all three pattern structures follows an upward trend, which is consistent with the findings of (F. Yang, Chen, et al., 2021; Tai et al., 2021). At a pattern height of 1 mm, the arc-shaped pattern structure generates the lowest maximum stalk pulling force, measured at 47.650 N. At a pattern height of 3 mm, the interlaced pattern structure generates the highest stalk pulling force, approximately 1.7 times greater than the lowest force observed for the arc-shaped pattern.

The analysis of variance ANOVA for the effects of pattern shape and pattern spacing on stalk pulling force is shown in Table 8. It can be observed that pattern shape, pattern spacing, and their interaction have a highly significant effect on stalk pulling force ($p < 0.01$). As pattern spacing increases, the stalk pulling force for inclined and arc-shaped patterns initially decreases and then stabilizes, while the stalk pulling force for interlaced patterns exhibits a sharp decline followed by a continuous upward trend. At a pattern spacing of 6.5 mm, the interlaced pattern structure generates the lowest stalk pulling force, measured at 61.725 N. At a pattern spacing of 5 mm, the interlaced pattern structure generates the highest stalk pulling force, approximately 2.15 times greater than the lowest value recorded.

Based on the above analysis, to enhance the stalk pulling force of the picking rollers while ensuring that stalk breakage does not occur during operation, the optimal structural parameters for each surface pattern are as follows.

Table 7

Analysis of variance ANOVA for the effects of pattern shape A and pattern height B on stalk pulling force.

Source	SS	df	MS	F值	P值
Pattern Shape A	205.505	2	102.753	512.482	<0.01
Pattern Height B	6191.364	4	1547.841	7719.906	<0.01
Pattern Shape A × Pattern Height B	140.690	8	17.586	87.712	<0.01
Error	9.023	45	0.201		

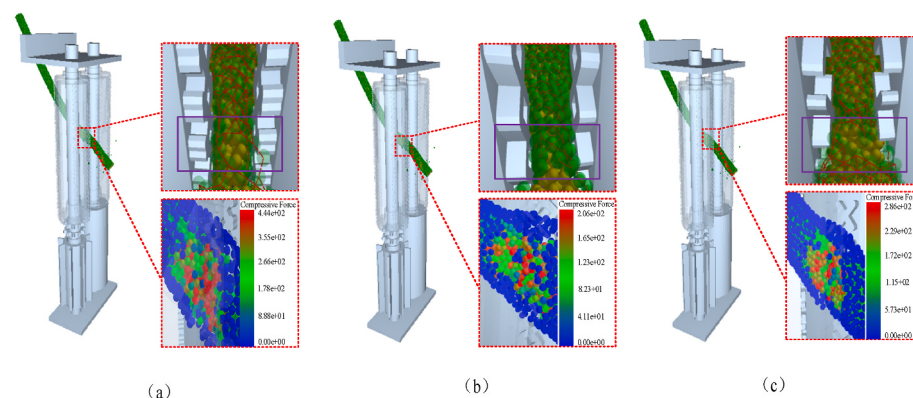


Fig. 13. Contact states between the stalk and different pattern spacings with a pattern height of 2.5 mm (a) contact state at a spacing of 5 mm (b) contact state at a spacing of 6.5 mm (c) contact state at a spacing of 11 mm.

Table 8

Analysis of variance ANOVA for the effects of pattern shape A and Pattern Spacing C on stalk pulling force.

Source	SS	df	MS	F值	P值
Pattern Shape A	2606.608	2	1303.304	5236.490	<0.01
Pattern Spacing C	11263.622	4	2815.906	11313.906	<0.01
Pattern Shape A × Pattern Spacing C	4099.387	8	512.423	2058.844	<0.01
Error	11.200	45	0.249		

- (i) Inclined pattern: At a pattern height of 2.5 mm and a pattern spacing of 8 mm, the maximum stalk pulling force achieved is 74.250 N.
- (ii) Interlaced pattern: At a pattern height of 2.5 mm and a pattern spacing of 8 mm, the maximum stalk pulling force achieved is 73.275 N.
- (iii) Arc-shaped pattern: At a pattern height of 2.5 mm and a pattern spacing of 6.5 mm, the maximum stalk pulling force achieved is 70.625 N.

The optimal pattern structure is an inclined pattern structure with a pattern height of 2.5 mm and a pattern spacing of 8 mm.

3.4. Validation of Simulation Results

In Section 3.3, the effects of picking roller surface structure (including pattern height, pattern spacing, and pattern shape) on stalk pulling force were analysed through simulation experiments, and the maximum stalk pulling forces corresponding to different surface structures were obtained. To validate the accuracy of the simulation analysis results, six sets of actual bench tests were conducted under identical conditions, and the maximum stalk pulling force values from the actual tests were obtained, as shown in Fig. 14. For the inclined pattern at a pattern height of 2.5 mm and a pattern spacing of 8 mm, the measured average maximum stalk pulling force was 76.110 N. For the interlaced pattern at a pattern height of 2.5 mm and a pattern spacing of 8 mm, the measured average maximum stalk pulling force was 70.650 N. For the arc-shaped pattern at a pattern height of 2.5 mm and a pattern spacing of 6.5 mm, the measured average maximum stalk pulling force was 67.820 N. The relative errors between the simulation and actual test results were 2.44 %, 3.7 %, and 4.1 %, respectively. The discrepancy is primarily caused by the difficulty in maintaining consistency in stalk attitude during the pulling process and the variations in internode diameter of the stalk. The test results confirm that the simulation and actual test

results are largely consistent, thereby validating the simulation analysis conclusions. The optimal surface structure of the picking roller was determined to be an inclined pattern structure with a pattern height of 2.5 mm and a pattern spacing of 8 mm.

4. Discussion

The results of this study show that the surface structure of the picking rollers can alter their gripping capacity on the stalk, thereby improving the effectiveness of vibration wave transmission along the stalk during the coupling process with the picking rollers, and enhancing the efficiency and reducing the damage of the picking operation. Based on the findings, increasing the pattern height along the roller edges can strengthen the compressing and gripping effect of the rollers on the stalk, which facilitates vibration wave transmission and improves the picking performance. However, with a further increase in pattern height, the average clearance between rollers becomes smaller, leading to excessive compression of the stalk. This not only raises the risk of stalk breakage but can also negatively affect the performance of the vibrating picking operation. In severe cases, stalk breakage may even cause clogging of the ear-picking cutting table, interrupting the picking process. When the pattern height remains constant, pattern spacing also has a significant impact on the compressive effect on the stalk and the efficiency of vibration wave transmission. As the spacing decreases, the rollers' compression on the stalk and the effectiveness of vibration wave transmission increase, which improves the picking performance. However, when the spacing becomes too small, although the compressive effect on the stalk is further enhanced, it also promotes the generation of stalk debris and leaf fibre fragments. These fragments may adhere to the roller surface, weakening the compression effect of the patterns on the stalk. Consequently, excessively small spacing reduces the gripping effectiveness on the stalk, diminishes the efficiency of vibration wave transmission, and lowers the overall picking capacity of the rollers. The type of surface pattern also exerts a substantial influence on the gripping capacity and the reliability of vibration wave transmission. Among the tested structures, inclined patterns oriented perpendicular to the stalk conveying direction exhibited the best gripping, compressing, and vibration transmission performance. This is because such patterns not only increase the friction coefficient between the roller surface and the stalk, but also provide resistance to stalk motion after it deforms and enters the pattern grooves, thereby improving gripping and vibration wave transmission, which enhances picking performance. In contrast, straight interlaced patterns, although theoretically expected to improve gripping and compression, result in some grooves being parallel to the stalk conveying direction due to the interlacing design. This reduces the gripping effectiveness and vibration transmission, ultimately lowering picking performance. For arc-shaped interlaced patterns, the theoretical performance is similar to that of the straight interlaced design. However, during the conveying process, the angle between the stalk conveying direction and the roller axis continuously changes, which creates an uncertain number of grooves parallel to the stalk conveying direction. This causes fluctuations in picking effectiveness during operation, reducing the stability of the vibrating picking performance.

Compared with the previously developed edge-shaped rollers without surface patterns by our research team, the present study demonstrates clear improvements in the effectiveness of vibration wave transmission, the stalk pulling force, and the operational reliability (Geng et al., 2019; Wang et al., 2018). This is because, under the same picking clearance, the patterned rollers in this study exerted less excessive compression on the stalks, thereby reducing the risk of stalk breakage during the clamping and conveying process. Moreover, once the deformed stalks entered the pattern grooves after compression, the patterns oriented perpendicular to the stalk conveying direction imposed substantial resistance to slippage, which enhanced the stability of stalk conveying. As a result, the stability of vibration wave transmission from the picking roller group to the maize stalks was improved,

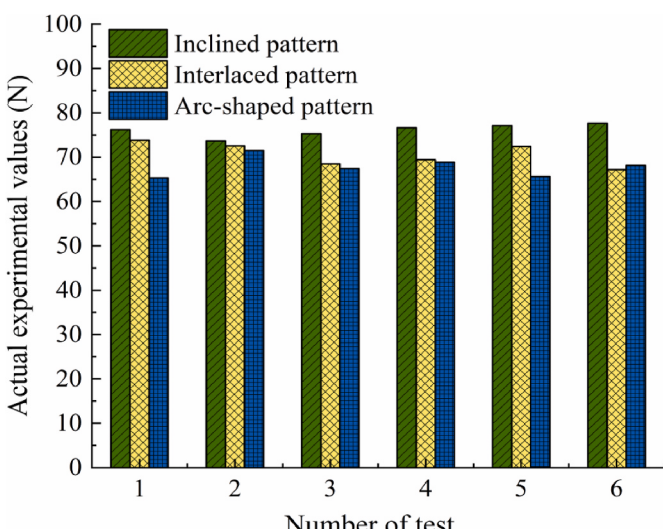


Fig. 14. Validation of simulation results.

creating favourable conditions for vibration-based picking and enhancing overall picking performance. In contrast, although the edge-shaped rollers without patterns could also generate vibration waves, excessively small picking clearances could lead to over-compression of thicker stalks, resulting in stalk breakage, loss of clamping stability, and ineffective vibration wave transmission, ultimately causing clogging of the rollers. Conversely, when the picking clearance was too large, thinner stalks could not be stably clamped, which reduced vibration transmission to the stalks, weakened the performance of vibration-based picking, and also increased the risk of roller clogging. Due to the improved gripping, compressive deformation, and pulling force characteristics provided by the patterned structures (Chen et al., 2025; F. Yang, Chen, et al., 2021), the risk of stalk breakage is significantly reduced while adaptability to thinner stalks is enhanced. If such patterned rollers were applied to longitudinal-horizontal roller picking devices, they could likewise improve the reliability and effectiveness of ear-picking cutting table operation. This provides a new perspective for the future development of maize vibration-based picking technologies.

In this study, a fixed feeding angle of 45° was adopted to ensure consistent comparison of different picking roller surface structures. However, this idealised assumption may not fully capture the complexity of actual harvesting conditions. In addition, certain operational conditions and biological factors, such as the rotational speed of the picking rollers, stalk moisture content, and variations in stalk diameter, were not considered. In practical harvesting operations, these factors can influence the mechanical properties of stalks and the pulling force, and their omission may affect the comprehensiveness of the present analysis. Future research will therefore consider different operational conditions and biological factors to further improve the comprehensiveness of the analysis. For example, incorporating roller rotational speed into the model will allow investigation of its interaction with surface structure parameters and provide insights into how rollers affect pulling performance under varying conditions. Similarly, stalk moisture content and diameter variation can be measured experimentally and parameterised in the stalk model to more realistically simulate stalk mechanical behaviour. By combining simulations with targeted bench tests and field trials, the effects of these factors and their interactions with roller surface structures can be systematically evaluated.

5. Conclusions

To address the issue of insufficient stalk pulling force in the vibratory maize picking device, this study employed a coupled simulation approach combining the Discrete Element Method (EDEM) and Multi-Body Dynamics (RecurDyn) to investigate the influence of picking roller surface structures on stalk pulling force, and determined the optimal surface structure parameters for maximizing the pulling force. The main conclusions are as follows.

- (1) To visually clarify the interaction between the vibratory picking device and maize stalks and to analyse the effect of roller surface structure on stalk pulling force, a DEM-MBD coupled simulation model of the picking device and stalk was developed. Maximum pulling force and power consumption were selected as evaluation indices. The simulation model was validated through bench tests. Under identical test conditions, the relative errors of the maximum pulling force and power consumption were 5.4 % and 5.2 %, respectively. These results indicate that the DEM-MBD simulation method can accurately model and analyse the interaction between the picking roller surface structure and maize stalks, verifying the reliability of the simulation model.
- (2) The DEM-MBD coupled model was used to analyse the influence of surface structure parameters on stalk pulling force. Simulation results showed that the pattern shape, pattern height, pattern spacing, and their interactions significantly affected the pulling

force. The optimal parameters for three types of surface structures were obtained: an inclined pattern structure with a height of 2.5 mm and a spacing of 8 mm; a staggered pattern structure with a height of 2.5 mm and a spacing of 8 mm; and an arc-shaped pattern structure with a height of 2.5 mm and a spacing of 6.5 mm. Among them, the inclined pattern structure produced the highest pulling force.

- (3) Bench tests were conducted to further verify the simulation results. The experimental results were generally consistent with the simulation outcomes, confirming the conclusions of the simulation analysis. To address the current issue of insufficient pulling force by picking rollers, selecting a roller with an inclined surface pattern of 2.5 mm height and 8 mm spacing can effectively enhance the pulling performance.

CRediT authorship contribution statement

Yipeng Cui: Writing – original draft, Methodology, Investigation, Data curation. **Pengxuan Guan:** Writing – original draft, Conceptualization. **Jianning Yin:** Writing – original draft, Investigation. **Zehao Zha:** Writing – review & editing, Software. **Qiming Yu:** Writing – review & editing, Data curation. **Zhenwei Wang:** Resources, Data curation. **Duanyang Geng:** Writing – original draft, Methodology, Funding acquisition, Conceptualization.

Declaration of competing interest

The authors declare that they have no known competing financial interests or personal relationships that could have appeared to influence the work reported in this paper.

Acknowledgements

This study was funded by the National Natural Science Foundation of China under Grant No. 32372008.

References

- Chen, M., Liu, X., Hu, P., Zhai, X., Han, Z., Shi, Y., Zhu, W., Wang, D., He, X., & Shang, S. (2024). Study on rotor vibration potato-soil separation device for potato harvester using DEM-MBD coupling simulation. *Computers and Electronics in Agriculture*, 218, Article 108638. <https://doi.org/10.1016/j.compag.2024.108638>
- Chen, J. Z., Shi, R. J., Zhao, W. Y., Dai, F., Zhao, Y. M., & Liu, X. L. (2025). Simulation and experiment of kernel loss during peeling of seed maize based on DEM-MBD coupling. *Biosystems Engineering*, 257.
- Chen, G., Wang, Q., Li, H., He, J., Wang, X., Zhang, X., & He, D. (2024). Experimental research on vertical straw cleaning and soil tillage device based on soil-straw composite model. *Computers and Electronics in Agriculture*, 216, Article 108510. <https://doi.org/10.1016/j.compag.2023.108510>
- Dong, W., Wu, Y., Liu, F., Hu, H., Yan, J., Bai, H., & Zhao, X. (2024). Design and experiment of a harvesting header for wide-narrow-row corn. *Applied Sciences*, 14 (3), 1309. <https://doi.org/10.3390/app14031309>
- Du, Y., Zhu, Z., Song, Z., Mao, E., & Li, F. (2012). Simulation of divider and snapping roll for small-scale maize harvester. *Transactions of the Chinese Society for Agricultural Machinery*, 43(S1), 100–105. <https://doi.org/10.6041/j.issn.1000-1298.2012.50.020> (in Chinese).
- Fang, W., Wang, X., Han, D., Zang, N., Chen, X., & Ohiemi, I. E. (2024). Parameter optimization and disturbance analysis of the film picking device of the chain-type plough layer residual film recovery machine based on DEM-MBD coupling. *Computers and Electronics in Agriculture*, 222, Article 109041. <https://doi.org/10.1016/j.compag.2024.109041>
- Fu, Q., Fu, J., Chen, Z., & Ren, L. (2023). Design and experimental study on a corn picking device based on the fracture mechanics of corn peduncle. *Journal of the ASABE*, 66(5), 1067–1076. <https://doi.org/10.13031/ja.15105>
- Gang, W., Honglei, J., Lie, T., Jian, Z., Ximeng, J., & Mingzhuo, G. (2016). Design of variable screw pitch rib snapping roller and residue cutter for corn harvesters. *International Journal of Agricultural and Biological Engineering*, 9(1), 27–34. <https://doi.org/10.3965/j.ijabe.20160901.1941>
- Geng, D., Wang, Q., Lu, X., Yu, X., Liu, Y., & Jin, C. (2019). Design and experiment on vertical polygonal roller snapping ears of corn harvester based on excitation theory. *Transactions of the Chinese Society for Agricultural Machinery*, 50(5), 124–132. <https://doi.org/10.6041/j.issn.1000-1298.2019.05.014> (in Chinese).
- He, D., Li, H., He, J., Lu, C., Wang, C., Wang, Y., Wu, Y., Tong, Z., & Gao, Z. (2025). Research on vibration characteristics of no-tillage seeding unit based on the MBD-

- DEM coupling. *Computers and Electronics in Agriculture*, 230, Article 109877. <https://doi.org/10.1016/j.compag.2024.109877>
- Jin, X., Chen, Z., Zhao, L., Zhao, B., Li, M., Zhou, L., & Ji, J. (2024). Optimization and testing of a mechanical roller seeder based on DEM-MBD rice potting tray. *Computers and Electronics in Agriculture*, 227, Article 109670. <https://doi.org/10.1016/j.compag.2024.109670>
- J. Shinnars, K. C., Boettcher, G. S., Hoffman, D. T., Munk, J. E., Muck, R., & J. Weimer, P. (2009). Single-pass harvest of corn grain and stover: Performance of three harvester configurations. *Transactions of the ASABE*, 52(1), 51–60. <https://doi.org/10.13031/2013.25940>
- Li, Z. Y., Fu, J., Luo, X. W., Fu, Q. K., Chen, Z., & Ren, L. Q. (2024). Determination of friction characteristics of corn ears at varying factors in mechanical peeling. *Journal of Food Process Engineering*, 47(11). <https://doi.org/10.1111/jfpe.14764>
- Li, T. Y., Guan, X. D., & Zhou, F. J. (2023). Mechanistic analysis and experimental study of shear-type low-loss fresh corn ear-picking mechanism. *Computers and Electronics in Agriculture*, 213. <https://doi.org/10.1016/j.compag.2023.108191>
- Li, Y., Tao, C., Zhe, Q., Kehong, L., Xiaowei, Y., Dandan, H., Bingxin, Y., Dongyue, Z., & Dongxing, Z. (2016). Development and application of mechanized maize harvesters. *International Journal of Agricultural and Biological Engineering*, 9(3), 15–28. <https://doi.org/10.3965/j.ijabe.20160903.2380>
- Lin, J., Liao, Q., Wang, X., Kang, Y., Du, W., & Zhang, Q. (2024). Exploring straw movement through the simulation of shovel-type seedbed preparation machine-straw-soil interaction using the DEM-MBD coupling method. *Computers and Electronics in Agriculture*, 226, Article 109465. <https://doi.org/10.1016/j.compag.2024.109465>
- Liu, L., Wang, X., Zhang, X., Cheng, X., Wei, Z., Zhou, H., & Zhao, K. (2023). The impact of 'T'-shaped furrow opener of no-tillage seeder on straw and soil based on discrete element method. *Computers and Electronics in Agriculture*, 213, Article 108278. <https://doi.org/10.1016/j.compag.2023.108278>
- Liu, L., Wang, X., Zhang, X., Zhong, X., Wei, Z., Geng, Y., Cheng, X., Zhao, K., & Bai, M. (2023). Determination and verification of parameters for the discrete element modelling of single disc covering of flexible straw with soil. *Biosystems Engineering*, 233, 151–167. <https://doi.org/10.1016/j.biosystemseng.2023.08.001>
- Liu, Y., Zhang, F., Song, X., Wang, F., Zhang, F., Li, X., & Cao, X. (2022). Study on mechanical properties for corn straw of double-layer bonding model based on discrete element method. *Journal of Northeast Agricultural University*, 53(1), 45–54. <https://doi.org/10.19720/j.cnki.issn.1005-9369.2022.01.006>
- Luo, H., Nie, J., & Zhang, L. (2023). Design and test of dislocation baffle roller bionic picking device for fresh corn. *Agriculture*, 13(5), 991. <https://doi.org/10.3390/agriculture13050991>
- Oduntan, Y., Kunduru, B., Tabaracci, K., Mengistie, E., McDonald, A. G., Sekhon, R. S., & Robertson, D. J. (2024). The effect of structural bending properties versus material bending properties on maize stalk lodging. *European Journal of Agronomy*, 159, Article 127262. <https://doi.org/10.1016/j.eja.2024.127262>
- Opheim, D. C. (1994). *Method of converting corn picker/husker to reduce kernel loss and damage: Google patents*.
- Qin, J. H., Yin, Y. P., Liu, Z. G., Du, Y. F., Wang, G. Y., Zhu, Z. X., & Li, Z. (2020). Optimisation of maize picking mechanism by simulation analysis and high-speed video experiments. *Biosystems Engineering*, 189, 84–98. <https://doi.org/10.1016/j.biosystemseng.2019.11.010>
- Rossi, R. J., & McGuire, P. C. (1992). *Method and apparatus for partially husking corn*. Google Patents.
- Seifi, M. R., & Alimardani, R. (2010). The moisture content effect on some physical and mechanical properties of corn (sc 704). *Journal of Agricultural Science*, 2(4), 125–134. <https://doi.org/10.5539/jas.v2n4p125>
- Shi, Y., Jiang, Y., Wang, X., Thuy, N. T. D., & Yu, H. (2023). A mechanical model of single wheat straw with failure characteristics based on discrete element method. *Biosystems Engineering*, 230, 1–15. <https://doi.org/10.1016/j.biosystemseng.2023.03.017>
- Tai, J., Li, H., Guan, Y., Ding, N., Du, Y., & Mao, E. (2021). Simulation of a maize ear picking device with a longitudinal horizontal roller based on hypermesh modeling. *Bioresources*, 16(1), 1394. <https://doi.org/10.1537/biores.16.1.1394-1410>
- Tang, H., Xu, C., Zhao, J., & Wang, J. (2023). Stripping mechanism and loss characteristics of a stripping-prior-to-cutting header for rice harvesting based on CFD-DEM simulations and bench experiments. *Biosystems Engineering*, 229, 116–136. <https://doi.org/10.1016/j.biosystemseng.2023.03.023>
- Wang, Q., He, K., Jin, C., Lu, X., Geng, D., & Zhang, G. (2018). Mechanism analysis and experiment optimization on parameters of maize exciting and picking. *Transactions of the Chinese Society for Agricultural Machinery*, 49(S1), 249–257. <https://doi.org/10.6041/j.issn.1000-1298.2018.S0.033> (in Chinese).
- Xiao, Z., Tian, H., Zhang, T., Wang, D., Sheng, Y., Li, D., Liu, F., & Zhou, J. (2022). Parameter calibration of discrete element numerical simulation for the dedusting sieve of corn straw feed. *Journal of China Agricultural University*, 27(7), 172–183. <https://doi.org/10.11841/j.issn.1007-4333.2022.07.16> (in Chinese).
- Xie, D., He, J., Liu, T., Liu, C., Zhao, G., & Chen, L. (2024). Establishment and validation the DEM-MBD coupling model of flexible straw-Shajiang Black soil-walking mechanism interactions. *Computers and Electronics in Agriculture*, 224, Article 109203. <https://doi.org/10.1016/j.compag.2024.109203>
- Xin, S., Zhao, W., Shi, L., Dai, F., Feng, B., Yan, Z., & Lyu, D. (2023). Design and experiments of the clamping and conveying device for the vertical roller type corn harvesting header. *Transactions of the Chinese Society of Agricultural Engineering*, 39 (9), 34–43. <https://doi.org/10.11975/j.issn.1002-6819.202211036> (in Chinese).
- Yang, R., Chen, D., Zha, X., Pan, Z., & Shang, S. (2021). Optimization design and experiment of ear-picking and threshing devices of corn plot kernel harvester. *Agriculture*, 11(9), 904. <https://doi.org/10.3390/agriculture11090904>
- Yang, F., Du, Y. F., Fu, Q. F., Li, X. Y., Li, Z., Mao, E. R., & Zhu, Z. X. (2021). Design and testing of seed maize ear peeling roller based on hertz theory. *Biosystems Engineering*, 202, 165–178. <https://doi.org/10.1016/j.biosystemseng.2020.12.014>
- Zhang, L., Yu, J., Zhang, Q., & Fang, X. (2023). Design and testing of a new bionic corn-ear-picking test device. *Applied Sciences*, 13(2), 838. <https://doi.org/10.3390/app13020838>
- Zhang, L., Yu, J., Zhang, Q., Liu, C., & Fang, X. (2022). Design and experimental study of bionic reverse picking header for fresh corn. *Agriculture*, 13(1), 93. <https://doi.org/10.3390/agriculture13010093>
- Zhu, G., Li, T., Zhou, F., & Wang, W. (2023). Design and experiment of bionic ear picking device for fresh corn. *Journal of Jilin University(Engineering and Technology Edition)*, 53(4), 1231–1244. <https://doi.org/10.13229/j.cnki.jdxgbxb.20210767> (in Chinese).